ACS APPLIED MATERIALS & INTERFACES

Research Article

www.acsami.org

Microwave-assisted Synthesis of Mesoporous Co_3O_4 Nanoflakes for Applications in Lithium Ion Batteries and Oxygen Evolution Reactions

Shuangqiang Chen,*,† Yufei Zhao,† Bing Sun,† Zhimin Ao,† Xiuqiang Xie,† Yiying Wei,† and Guoxiu Wang*,†,‡

†Centre for Clean Energy Technology, School of Chemistry and Forensic Science, University of Technology Sydney, 15 Broadway, 2007, Sydney, New South Wales, Australia

‡College of Material Science & Engineering, Nanjing University of Aeronautics and Astronautics, Nanjing, P. R. China

Supporting Information

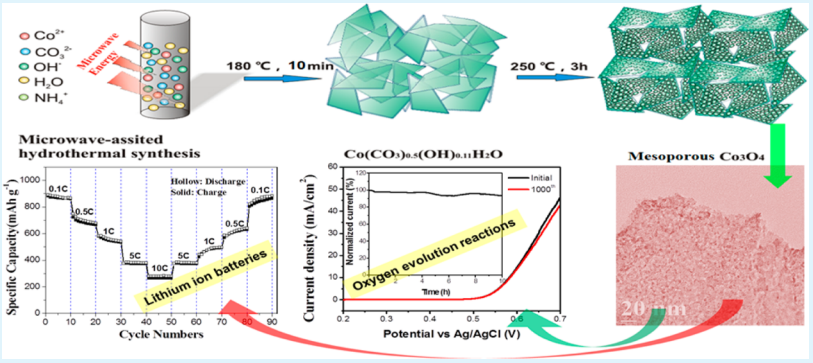

ABSTRACT: Mesoporous Co_3O_4 nanoflakes with an interconnected architecture were successfully synthesized using a microwave-assisted hydrothermal and low-temperature conversion method, which exhibited excellent electrochemical performances as anode materials in lithium ion batteries and as catalysts in the oxygen evolution reaction (OER). Field-emission scanning electron microscopy (FESEM) and transmission electron microscopy (TEM) observations showed the unique interconnected and mesoporous structure. When employed as anode materials for lithium ion batteries, mesoporous Co_3O_4 nanoflakes delivered a high specific capacity of 883 mAh/g at 0.1C current rate and stable cycling performances even at higher current rates. Post-mortem analysis of *ex situ* FESEM images revealed that the mesoporous and interconnected structure had been well maintained after long-term cycling. The mesoporous Co_3O_4 nanoflakes also showed both OER active properties and good catalytic stability. This could be attributed to both the stability of unique mesoporous structure and highly reactive facets.

KEYWORDS: *mesoporous structure, Co_3O_4 nanoflakes, microwave synthesis, lithium ion batteries, oxygen evolution reactions*

1. INTRODUCTION

Energy storage has been substantially researched and applied in recent decades, including traditional rechargeable batteries (lead-acid batteries, nickel−cadmium batteries, and nickel−metal hydride batteries) and lithium-ion batteries.[1−4] Due to toxic materials, self-discharge, and the memory effect of traditional batteries, lithium ion batteries are regarded as the most promising energy storage devices. For commercial lithium ion batteries, graphite with a theoretical capacity of 372 mAh/g cannot meet the current requirements of high capacity, long cycling life, and excellent tolerance of fast charge/discharge.[5−7] Recently, many efforts have been devoted to developing good electrochemical performances of anode materials, including carbon based materials, Si, Sn, and various transition metal oxides.[8−17] Among those transition metal oxides, Co_3O_4 has been recognized as one of the promising materials because of its high theoretical capacity of 890 mAh/g in lithium-ion batteries and multiple usages in supercapacitors and Li−O_2 batteries.[18−22] However, Co_3O_4 is also plagued by low rechargeable capacity and fast capacity decay due to the large volume expansion, electrode pulverization, and unstable solid electrolyte interphase (SEI) during charging. It should be noted that morphology and nanostructure have large influences on the electrochemical performances.[23−26] High specific capacity at high current density and long cycling performance of mesoporous and hollow Co_3O_4 nanospheres due to the reactivation process and stabilized SEI layer have been recently reported.[25] The mesoporous and hollow Co_3O_4 nanomaterials wrapped by highly conductive and light graphene nanosheets are illustrated to deliver high capacity and exceptional

Received: November 19, 2014
Accepted: January 13, 2015
Published: January 13, 2015

DOI: 10.1021/am508136k
ACS Appl. Mater. Interfaces 2015, 7, 3306−3313

cyclability due to the synergistic effect.[18,26,27] Moreover, it is demonstrated that crystal plane structures of Co_3O_4 have a critical impact on the lithium ion storage and cycling performances, showing that the (110) plane of Co_3O_4 is ideal for lithium ion batteries, compared with other facets. Liu et al. has reported unusual single-crystal Co_3O_4 nanocages with highly reactive {110} facets via the hydrothermal method, followed with the treatment of H_2O_2, demonstrating a high reversible capacity of 864 mAh/g at 0.2C over 50 cycles.[28] Many reports also illustrate that Co_3O_4 with different morphologies including nanotubes, nanorods, nanoneedles, nanowires, platelets, and mesoporous structures have enhanced capacities and better cycle life than bulk materials.[27,29−33]

Water splitting is an efficient way to generate hydrogen in high purity, but it needs stable and effective catalysts to drive water oxidation into molecular oxygen.[19,34−37] The corresponding oxygen evolution reaction (OER) plays a critical role in the process of water splitting.[38−40] Despite substantial efforts having been devoted to developing the effective catalysts for OER, it remains a great challenge without using noble metal catalysts. Although the oxides of ruthenium, iridium, and other rare earth metals in high oxidation states were tested to be effective catalysts for OER, the high price of those metal oxides makes them impossible for practical large-scale applications. Cobalt oxides and other transition metal oxides with different morphologies are also active for oxygen evolution reactions in an alkaline solution.[41−43] Esswein et al. discovered that the sizes of Co_3O_4 had different catalysis abilities on OER, illustrating that the current density of 10 mA/cm^2 of cubic nanoparticles with an average diameter of 5.9 nm was achieved at an overpotential of 328 mV.[44] Wu et al. reported that the Co_3O_4 nanocrystal anchored on a single-walled carbon nanotube, synthesized via a self-assembly approach, exhibited much enhanced catalytic activity and excellent stability under both neutral and alkaline solutions.[45]

Herein, we report mesoporous Co_3O_4 nanoflakes with an interconnected architecture synthesized by a microwave-assisted hydrothermal and low-temperature conversion method, which exhibits excellent electrochemical performances as anode materials in lithium ion batteries and as catalysts in OER under alkaline solutions. FESEM and TEM analyses show the unique interconnected and mesoporous structure. When employed as anode materials for lithium ion batteries, mesoporous Co_3O_4 nanoflakes delivered a high specific capacity of 883 mAh/g at a 0.1C current rate and stable cycling performance. The mesoporous Co_3O_4 nanoflakes also show both OER active property and good catalytic stability, even cycled 1000 times. This could be attributed to both the stability of the unique mesoporous structure and exposed highly reactive energy facets on the edges

2. EXPERIMENTAL SECTION

2.1. Preparation of Mesoporous Co_3O_4 with Microwave-Assisted Method. In a typical synthesis, ethylene glycol (20 mL), hexamethylenetetramine aqueous solution (8 mL, 0.06 M), ammonium carbonate aqueous solution (8 mL, 0.06 M), and cobalt(II) carbonate aqueous solution (10 mL, 0.08 M) were mixed under vigorous stirring to obtain a homogeneous purple solution. Once the precursor was transferred to a glass vessel with a volume of 23 mL, a thermal treatment was performed in a single-mode microwave synthesizer (NOVA II microwave synthesizer with magnetron stirring and monitoring the real pressure in the vessel) at 180 °C for 10 min. After cooling to room temperature, the sample deposited at the bottom was collected and washed using a filtration apparatus with copious deionized water (D.I. water) and ethanol. The as-synthesized sample was dried in a vacuum oven at 80 °C overnight to remove the absorbed water for the subsequent characterizations. Then, the dried precursor was annealed at 250 °C for 3 h with a temperature ramp rate of 2 °C/min.

2.2. Materials Characterization. The as-prepared mesoporous Co_3O_4 with interconnected structure was characterized using X-ray diffraction (Rigaku D/max-2550 V with Cu Kα radiation) operated at 40 kV and 30 mA. Raman spectra were measured using a Renishaw inVia Raman spectrometer system (Gloucestershire, UK) equipped with a Leica DMLB microscope (Wetzlar, Germany) and a 17 mW at 633 nm Renishaw helium neon laser with 50% power. Nitrogen adsorption−desorption measurements were conducted on a 3 Flex surface characterization analyzer to determine the Brunauer−Emmett−Teller (BET) specific surface areas using a Quadrasorb SI analyzer at 77 K. The BET surface area was calculated using experimental points at a relative pressure of P/P_0 = 0.05−0.25. The pore size distribution was derived from the desorption branch using the Barrett−Joyner−Halenda (BJH) method. The morphologies and crystal structure of materials were analyzed using a field emission scanning electron microscope (JSM-6700F, 20 kV) and a transmission electron microscope (TEM, JEOL JEM-200CX and JEM-2010F)

2.3. Electrochemical Measurements. The working electrodes were made from 80% of active materials, 10% of the conductive agent (acetylene black), and 10% of the binder (polyvinylidene difluoride). The mixture was stirred with an adjustable high-speed electric agitator. The working electrodes were dried in a vacuum oven. CR2032 coin cells were assembled in an argon-filled glovebox (Mbraun, Unilab, Germany), in which both the moisture and oxygen contents were controlled to be less than 0.1 ppm. Lithium foil was used as a counter electrode. The electrolyte was 1 M $LiPF_6$, which dissolved in a 1:1 (weight ratio) mixture of ethylene carbonate and diethyl carbonate. Electrochemical measurements were performed using a LAND-CT2001C battery test system. The cells were discharged and charged galvanostatically in the fixed voltage range of 0.01−3 V with a current density of 89 mA/g (0.1C). Higher current rates (0.5C, 1C, 5C, and 10C) were also applied to test the electrochemical performances. After 300 cycles, the electrode materials were taken from the coin cells in the glovebox and washed by ethylene carbonate to remove the contained electrolyte. The cycled electrode materials were analyzed by SEM.

2.4. Measurement of Oxygen Evolution Reaction. Electrocatalytic activity measurement was carried out on a CH instrument Model 600E electrochemical workstation with a three-electrode glass cell in 1 M KOH. Glass carbon (GC) was the sample used as the working electrode, while the platinum wire and the Ag/AgCl electrode were the counter and the reference electrodes. The working electrode was prepared as follows: 4 mg of the Co_3O_4 was dispersed in 1 mL of 1:1 v/v water/isopropanol, and then 80 μL of 5 wt % Nafion was added to the solution. The mixture was sonicated for more than 30 min to obtain a homogeneous ink. Then, 10 μL of the catalyst ink was loaded onto a GC electrode of 5 mm in diameter. Linear sweep voltammetry was conducted with a scan rate of 5 mV/s. The working electrode is measured on the rotating disk produced by Pine Research Instrumentation and controlled by a rotating electrode speed control (0−3000 rpm). To test the stability of electrode, multiple-cycle measurements (1000 cycles) can be controlled by the software (CHI660D Electrochemical Workstation) via the "Repetitive Runs" function. Electrochemical impedance spectroscopy (EIS, 0.1 Hz-100 kHz, 10 mV) is measured on a CHI 660E electrochemical workstation (CH instrument, Inc.) at room temperature.

3. RESULTS AND DISCUSSION

3.1. Preparation and Structural Characterization of Mesoporous Co_3O_4 Nanoflakes. The mesoporous Co_3O_4 nanoflakes with interconnected architecture were synthesized by a microwave-assisted hydrothermal and low-temperature conversion method. This approach has been widely applied to the preparation of various nanomaterials and even industrial

DOI: 10.1021/am508136k
ACS Appl. Mater. Interfaces 2015, 7, 3306−3313

Scheme 1. Schematic Illustration of the Microwave-assisted Hydrothermal Synthesis of Mesoporous Co_3O_4 Nanoflakes

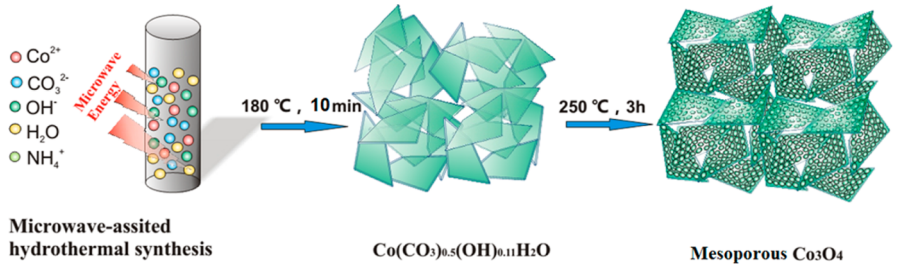

productions because of its advantages, such as being less time-consuming, having simple operation, and having energy efficiency. A schematic diagram of the synthesis procedure is presented in Scheme 1. With the assistance of microwave energy and high pressure (~4 atm), layered intermediate cobalt carbonate hydroxide hydrates ($Co(CO_3)_{0.5}(OH)_{0.11}H_2O$) with interconnected architectures are formed, assisted by the bihydroxyl functional group from ethylene glycol. After treatment at 250 °C in air, layered $Co(CO_3)_{0.5}(OH)_{0.11}H_2O$ releases carbon dioxide and moisture. After that, mesoporous Co_3O_4 nanoflakes with interconnected architecture are obtained.

The as-synthesized materials were characterized by X-ray diffraction (XRD) and are shown in Figure 1a. The intermediate is indexed to be cobalt carbonate hydroxide hydrates ($Co(CO_3)_{0.5}(OH)_{0.11}H_2O$) (JCPDS: 48−0083, a = 8.792), and the final product is confirmed to be Co_3O_4 with typical characteristic peaks of (020), (311), (400), (511), and (440).[46] The positions and intensities of diffraction peaks match well with the standard JCPDS card (42−1467 with a space group of Fd3m (227), a = 8.084). Figure 1b shows the Raman spectrum of mesoporous Co_3O_4 nanoflakes. The peaks of Raman shift at 194, 518, and 617 cm^{-1} can be assigned to the F_{2g} mode of Co_3O_4, and the peaks at 475 and 682 cm^{-1} are ascribed to the E_g and A_{1g} modes of Co_3O_4, respectively. Values of the Raman shift are slightly different from those in the previous reports,[47] which is probably due to different sizes and morphologies of Co_3O_4 nanoflakes. The surface areas of mesoporous Co_3O_4 nanoflakes were investigated using nitrogen adsorption and desorption isotherms, as shown in Figure 1c. The mesoporous Co_3O_4 nanoflakes have a relatively high specific surface area of 139.8 m^2/g with a hysteresis feature, which is much larger than that of the $Co(CO_3)_{0.5}(OH)_{0.11}H_2O$ nanohydrates (19 m^2/g, shown in Figure S1). It indicates that many voids are formed on the planes of the Co_3O_4 nanoflakes during the heat treatment process. The total pore volume of the mesoporous Co_3O_4 nanoflakes was determined to be 0.346 cm^3/g, and the average pore size (inset image in Figure 1c) was approximately 11.5 nm, based on the Barrett−Joyner−Halenda method. This mesoporous and interconnected nanostructure can not only provide many reactive sites for lithium storage and enhance the electrolyte diffusion for lithium ions transport but also offer active planes for the OER activities.

Figure 2 shows the field-emission scanning electron microscopy (FESEM) images of the intermediate ($Co(CO_3)_{0.5}(OH)_{0.11}H_2O$) and mesoporous Co_3O_4 nanoflakes. It can be observed from Figure 2a and b that the cobalt carbonate hydroxide hydrates arrange themselves into a thin plate structure with a thickness of ~20 nm, which is probably ascribed to the assistance of ethylene glycol. Double-headed hydroxyl groups in ethylene glycol molecules can intercalate

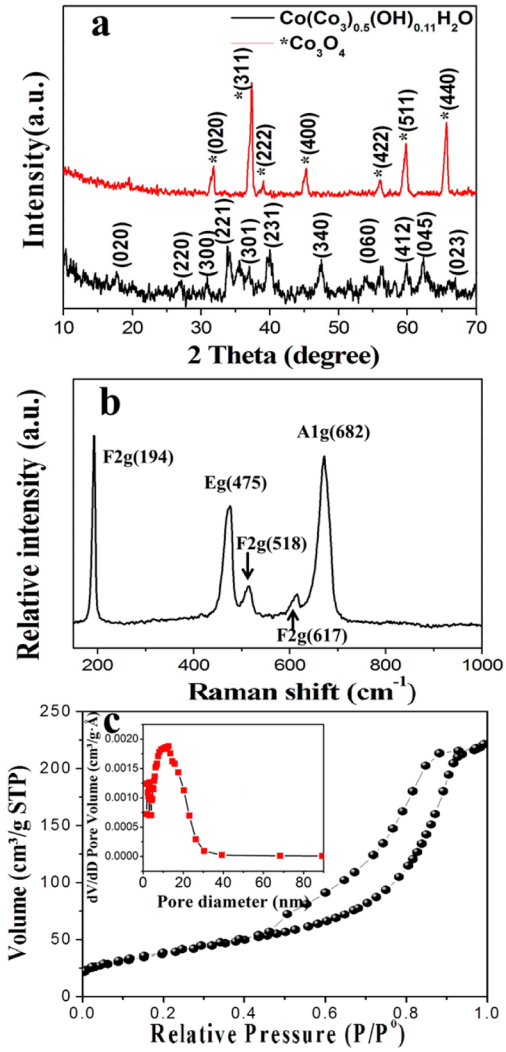

Figure 1. Structural analysis of Co_3O_4 and its intermediate. (a) X-ray diffraction pattern of intermediate $Co(CO_3)_{0.5}(OH)_{0.11}H_2O$ and Co_3O_4. (b) Raman spectrum of Co_3O_4. (c) Nitrogen adsorption and desorption isotherms of mesoporous Co_3O_4 nanoflakes with the inset plot of pore size distribution.

into neighboring layers and act as soft templates to assist the formation of interconnected layered architecture. Previous reports also mentioned that ethylene glycol molecules act as molecular pillars to separate and stabilize a layered intermediate via hydrogen bonding action, resulting in the formation of layered structures.[24,25] This morphology is similar to layered double-metal hydroxides (LDH), which contain an anion of carbonate or hydroxyl groups. Meanwhile, the strong microwave absorption of ethylene glycol molecules results in severe

DOI: 10.1021/am508136k
ACS Appl. Mater. Interfaces 2015, 7, 3306−3313

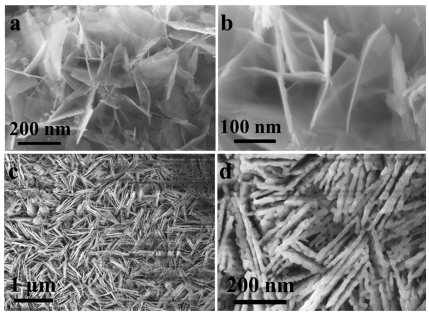

Figure 2. Morphologies characterizations. Low and high magnification of field-emission scanning electron microscopy (FESEM) images of $Co(CO_3)_{0.5}(OH)_{0.11}H_2O$ (a and b). Low and high magnification FESEM images of Co_3O_4 with mesoporous structure (c and d).

stretching vibrations, leading to partially disordered layered planes and forming an interconnected, three-dimensional architecture. Those anions of carbonate, hydroxyl, or other groups on the interconnected structure are thermally sensitive, which tends to emit gases including carbon dioxide, moisture, and ammonium molecules under subsequent thermal treatment. Mesoporous architecture can be generated upon the remaining metal oxides, which is a general strategy to achieving mesoporous structures originating from LDH compounds. Single-layered nanomesh, nanoparticles, nanoplates, and nanobelts have also been successfully obtained by means of the unique physical and chemical instability of LDH compounds.[48]

Inspired by this strategy, the intermediate $Co(CO_3)_{0.5}(OH)_{0.11}H_2O$ was slowly heated in the air at 250 °C for 3 h. The release of carbon dioxide, ethylene glycol, and moisture from layered planes upon the precursor's thermal decomposition leaves copious amounts of mesoporous voids,[46] which have been verified by the BET measurement in Figure 1c and FE-SEM images in Figure 2c,d. Meanwhile, the unique interconnected architecture of the intermediate is also completely maintained, which is demonstrated by the typical low and high magnification of FESEM in Figure 2c-d and Figure S2a-b. The FESEM images clearly show the uniformity, interconnected property, and regularity of mesoporous Co_3O_4 nanoflakes. It should be noted that the overall size of interconnected mesoporous Co_3O_4 nanoflakes is more than 30 μm, indicating that more than hundreds of square meters are obtained by this effective microwave-assisted and thermal decomposition method. Interestingly, the planes of mesoporous Co_3O_4 nanoflakes connect themselves in a continuously end-to-end manner, which substantially increases the mechanical strength and overall stability. Several mesoporous Co_3O_4 nanoflakes with a thickness of around 15 nm enclose extra voids. The average voids are approximately 11.5 nm, providing enough space for the subsequent volume expansion when applied as anode materials for lithium ion batteries and extra space for oxygen evolution reaction.

The mesoporous architecture and crystal structure of interconnected Co_3O_4 nanoflakes were further characterized by transmission electron microscopy (TEM) and high resolution TEM (HR-TEM). From Figure 3a,b, it is observed that the planes of Co_3O_4 nanoflakes consist of many mesopores. More TEM images of porous Co_3O_4 nanoflakes are presented in Figure S3a and b. The inset image in Figure 3b shows the enlarged view of mesoporous Co_3O_4 nanoflakes. As observed from Figure 3c, lattice distance agrees well with the {220}[27] facet of the face-centered-crystal Co_3O_4 and its

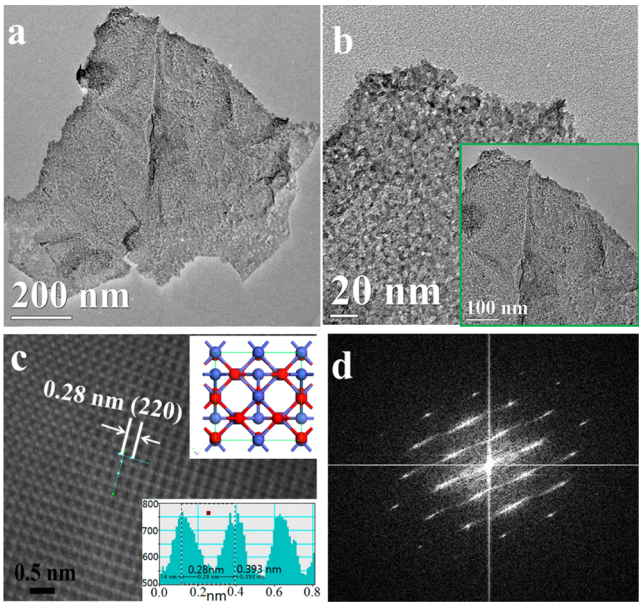

Figure 3. Structural characterizations. (a) Low magnification TEM image and (b) high resolution TEM (HR-TEM) image of mesoporous Co_3O_4 nanoflakes with an enlarged view. (c) HR-TEM image and the corresponding lattice profile of the (220) plane and its corresponding simulation scheme. (d) The relevant fast Fourier transform (FFT) pattern.

corresponding lattice profile. The other inset image in Figure 3c exhibits a structure stimulation of the (220) plane in the same direction, demonstrating the arrangement of cobalt and oxygen atoms. The corresponding fast Fourier transform (FFT) pattern is shown in Figure 3d.

3.2. Electrochemical Measurements on Lithium Ion Batteries. The electrochemical performances of mesoporous Co_3O_4 nanoflake electrodes with the interconnected architecture were evaluated using CR2032 coin cells by galvanostatic charge−discharge. The charge/discharge profiles of the mesoporous Co_3O_4 nanoflakes in the first, 100th, and 300th cycle are shown in Figure 4a at a constant current density (89 $mA{\cdot}g^{-1}$, 0.1C). The charge−discharge curves exhibit typical characteristic electrochemical behaviors of Co_3O_4 nanoflake electrodes. In the first cycle, the mesoporous Co_3O_4 nanoflake electrode delivered a discharge capacity of 1192 mAh/g, which is higher than the theoretical specific capacity (890 mAh/g).[18,49] The extra capacity is probably attributed to the formation of the solid electrolyte interphase (SEI) layer and contribution from nanocavities. The initial reversible capacity is 883 mAh/g with a Coulombic efficiency of 74%. The following specific capacities, such as 100th and 300th, exhibit no obvious capacity degradation. The corresponding electrochemical impedance spectra (EIS) were also measured before and after the 100th and 300th cycles in Figure S4, and the corresponding equivalent circuit is inserted in Figure S4, which reveals the changes of electrochemical resistances and the differences of charge transfer efficiencies. All three stages present Nyquist plots, which consist of a depressed semicircle in high frequency region and an oblique line in the medium frequency region. The small diameter (~85 ohm) of the semicircle in the high frequency region of fresh cell indicates a low electrochemical reaction resistance and small charge transfer impedance. However, the relative larger diameters (~102 ohm and ~220 ohm, respectively) of the other two semicircles after the 100th

DOI: 10.1021/am508136k
ACS Appl. Mater. Interfaces 2015, 7, 3306−3313

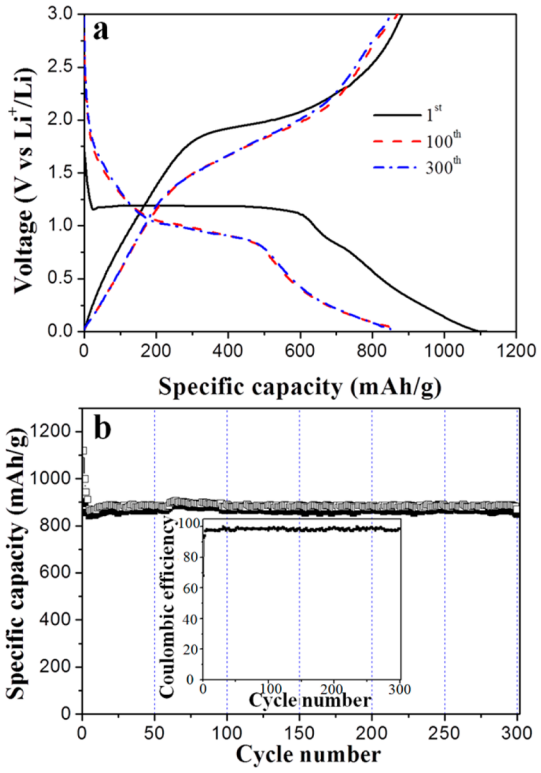

Figure 4. The electrochemical performance of mesoporous the Co_3O_4 nanoflakes electrode. (a) Galvanostatic charge/discharge profiles cycled at the first, 100th, and 300th between 0.01 and 3 V (vs Li^+/Li) at a current density of 89 mA/g (0.1C). (b) Cycling performance of the mesoporous Co_3O_4 electrode and its Coulombic efficiency at 0.1C as inset image.

and 300th cycles illustrate that after long cycles, the electrochemical resistances have slightly increased, verifying that the good stability of the SEI layer and low ohmic internal resistance changes during cycles. That might account for the high reversible capacity of mesoporous Co_3O_4 nanoflakes. The cycling performance, together with the corresponding Coulombic efficiency, as seen in the inset image in Figure 4b, exhibits a stable and long cycling life. After 300 cycles, the reversible capacity still maintains at 806 mAh/g with a capacity decay ratio about 0.1% per cycle. These results demonstrate that the mesoporous Co_3O_4 nanoflakes with interconnected architecture can sustain long cycling life testing.

Mesoporous Co_3O_4 electrodes were also measured at stepwise current densities: from 0.1C, 0.5C, 1C, and 5C, to 10C, and then reversed to low current rates. The electrochemical performances are presented in Figure 5a. The capacity of the mesoporous Co_3O_4 electrodes shows considerable stability, even when the current rates step-wisely increased. When the current rate reversed to a low current rate, the capacity of the mesoporous Co_3O_4 nanoflake electrode nearly recovered to the initial value. This result illustrated that the interconnected mesoporous Co_3O_4 nanoflake electrode can tolerate changes of current rates. The charge/discharge profiles and cycling performances of the mesoporous Co_3O_4 nanoflake electrodes at high current rates of 0.5C, 1C, 5C, and 10C are shown in Figure 5b and c, respectively. After 300 cycles, the reversible specific capacity of the mesoporous Co_3O_4 nanoflakes electrode at 0.5C (445 mA/g) maintained 686 $mAh \cdot g^{-1}$. The electrodes achieved specific capacities of 548 mAh/g at 1C (890 mA/g), 380 mAh/g at 5C (4450 mA/g), and 285 mAh/g at 10C (8900 mA/g). Aiming to investigate the mechanism of the achieved excellent performance of mesoporous Co_3O_4 nanoflakes, post-mortem analysis was conducted on the cycled electrode by *ex-situ* FE-SEM imaging. Figure S5a and b show the low and high magnification FE-SEM images of mesoporous Co_3O_4 nanoflakes after 300 cycles at 10C. Thin SEI are formed on the mesoporous Co_3O_4 nanoflake electrode after cycling, and more mesopores are generated in the hollow structure, leading to the formation of interconnected flower-like nano-

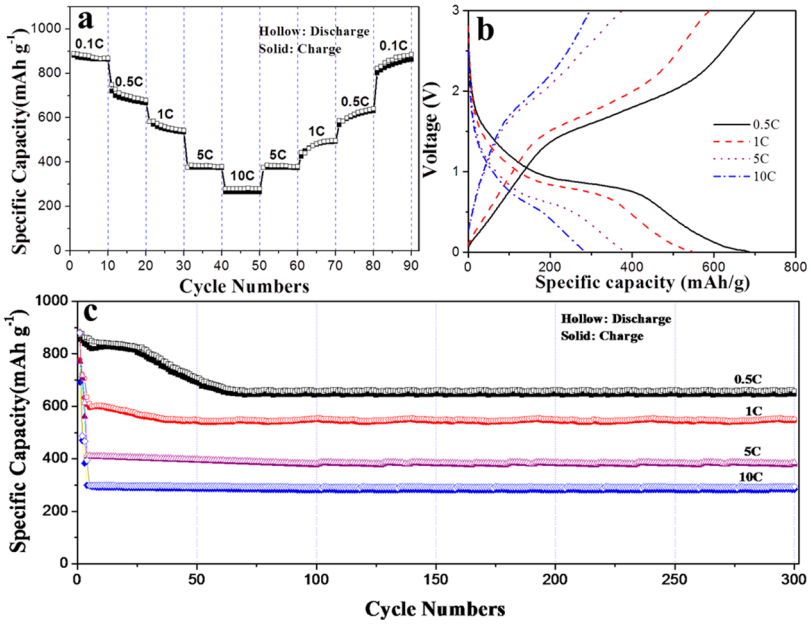

Figure 5. Electrochemical performances at high rates. (a) Stepwise rate performances at different current densities. (b) The galvanostatic charge/discharge profiles of mesoporous Co_3O_4 nanoflake electrodes at 0.5C, 1C, 5C ,and 10C at 300th cycle. (c) Cycling performances of mesoporous Co_3O_4 nanoflake electrodes at high current densities.

DOI: 10.1021/am508136k
ACS Appl. Mater. Interfaces 2015, 7, 3306−3313

sheets a few nanometers in thinkness, which are favorable to fast transport of lithium ions and electrons. The stable SEI layer and mesopores on electrodes can stabilize lithiation/delithiation and mitigate the mechanical degradation originating from large volume expansion during discharge. An enlarged view of the electrode after cycles is inserted in Figure S5b to demonstrate the well-maintained interconnected and flower-like Co_3O_4 nanosheets, which are beneficial to the reactivation mechanism and exceptional cyclabilities for electrodes at higher current densities.[25] Even though the cycled electrode is covered by SEI layers, the unique interconnected architecture can still be identified. Moreover, the mesoporous architecture is also a benefit for the distribution of electrolytes and transport of lithium ions. Therefore, mesoporous Co_3O_4 nanoflakes can exhibit both enhanced high capacity and good cyclability.

3.3. Electrochemical Measurements on Oxygen Evolution Reaction. Cobalt oxides and other transition metal oxides with different morphologies have demonstrated to be active for oxygen evolution in an alkaline solution.[20,43,50−54] Mesoporous Co_3O_4 nanoflakes with the interconnected architecture are rarely studied. In order to explore other potential applications for mesoporous Co_3O_4 nanoflakes, it is also evaluated as a catalyst for the oxygen evolution reaction (OER). The performance of mesoporous Co_3O_4 toward water oxidation was measured in a standard three-electrode system in the 1 M KOH solution, and the working electrode was continuously rotating at 1600 rpm to remove the generated oxygen bubbles. The commercial Co_3O_4 was also measured under the same testing conditions for comparison. The anode measured potentials vs Ag/AgCl were converted to the normal hydrogen electrode (NHE) according to Nernst equation $E_{NHE} = E_{Ag/AgCl} + 0.059 \times pH + 0.2224$. In 1 M KOH, the anodic current density of mesoporous Co_3O_4 nanoflakes, as shown in Figure 6a, showed an onset potential toward OER of 0.452 V (vs. Ag/AgCl) where the OER activity began and afforded a current density of 10 mA/cm^2 at a small overpotential of 380 mV. For the commercial Co_3O_4, the overpotential shifted to 451 mV when the current density reached 10 mA/cm^2. This outcome is comparable to the best performance of the previously reported Co_3O_4 toward the OER under the same conditions.[45]

In order to further demonstrate the high activity of the Co_3O_4 nanoflakes, Tafel plots of the two electrodes were obtained from the equation $\eta = b \log(j/j_0)$.[52,55] As shown in Figure 6b, mesoporous Co_3O_4 nanoflakes exhibited a Tafel slope of a = 48 mV/decade in 1 M KOH, while the commercial Co_3O_4 showed the Tafel slope of b = 59 mV/decade. This value of mesoporous Co_3O_4 nanoflakes is also smaller than that of Co_3O_4/graphene,[53] which implies that the synthesized mesoporous Co_3O_4 nanoflakes are a more efficient catalyst toward the OER. The high performance was further confirmed by impedance measurements in 1 M KOH (Figure 6c). The mesoporous Co_3O_4 nanoflake-modified GC electrode displayed much lower impedance than that of the commercial Co_3O_4. Therefore, much faster electron transfer between the mesoporous Co_3O_4 nanoflakes and the electrode substrate is one of the important factors contributing to the superior OER kinetics.[56,57]

The stability of the electrode in a long period is extremely important for practical applications. The stability of mesoporous Co_3O_4 nanoflakes was assessed for 1000 cycles (as shown in Figure 6d). The mesoporous Co_3O_4 nanoflakes exhibit good catalytic stability during the OER test, and no

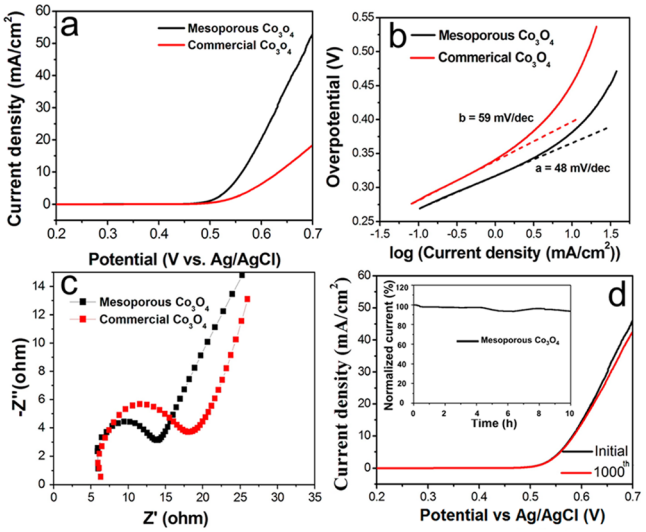

Figure 6. Electrochemical performances of mesoporous Co_3O_4 nanoflakes (black) and commercial Co_3O_4 (red) on oxygen evolution reaction. (a) The electrochemical performances on the oxygen evolution reaction of mesoporous Co_3O_4 and commercial Co_3O_4 swept from 200 to 900 mV vs Ag/AgCl at 5 mV/s in 1 M KOH aqueous solution. (b) Tafel plot (overpotential versus log current density) of commercial Co_3O_4 and mesoporous Co_3O_4 nanoflakes derived from a. (c) The electrochemical impedance spectra of commercial Co_3O_4 and mesoporous Co_3O_4 nanoflakes. (d) OER polarization curves for the mesoporous Co_3O_4 nanoflakes electrode in the first and 1000th cycle of accelerated stability test with an inset image of the chronoamperometric response of mesoporous Co_3O_4 nanoflakes (percentage of current retained versus operation time at 0.6 V in 1 M KOH electrolyte).

obvious decay of the activity is observed after 1000 cycles, demonstrating the considerably stable activity to OER. To further investigate the stability of the mesoporous Co_3O_4 nanoflakes in OER, a more than 10 h chronoamperometric measurement of mesoporous Co_3O_4 nanoflakes is conducted with the applied potential at +0.6 V (vs. Ag/AgCl, inset image in Figure 6d).[58] The stable current of the material further demonstrated the good stability (with a high retained ratio of 95.3%). The high stability of the mesoporous Co_3O_4 nanoflakes could be attributed to the stability of the unique mesoporous and interconnected structure.

In order to investigate the property of mesoporous Co_3O_4 for OER, a post-mortem analysis was also performed on the electrode after 1000 cycles using *ex situ* FE-SEM observations. Figure S6 exhibits the low and high magnification FE-SEM images of mesoporous Co_3O_4 material after OER measurement. It should be noted that even though the mesoporous Co_3O_4 nanoflakes have experienced 1000 cycles, the mesoporous structure and interconnected feature are still well maintained, providing solid evidence of the robust structural stability and superior electrochemical catalysis effect on the oxygen evolution reaction. The results indicate that the mesoporous Co_3O_4 nanoflakes with unique architecture can resist the strong causticity of alkaline conditions and microforces generated from oxygen bubbles.

4. CONCLUSION

In summary, we have successfully synthesized mesoporous Co_3O_4 nanoflakes with interconnected architecture using a microwave-assisted hydrothermal and low-temperature con-

DOI: 10.1021/am508136k
ACS Appl. Mater. Interfaces 2015, 7, 3306−3313

version method. The as-prepared materials exhibit excellent electrochemical performances as anode materials in lithium ion batteries and as catalysts for the oxygen evolution reaction in alkaline solutions. FESEM and TEM analyses show the unique interconnected and mesoporous structure. When employed as anode materials for lithium ion batteries, mesoporous Co_3O_4 nanoflakes delivered a high specific capacity of 883 mAh/g at 0.1C, and stable cycling performances at higher current rates. The mesoporous Co_3O_4 nanoflakes also exhibit catalytic activity toward OER, showing an onset potential of 0.452 V (vs. Ag/AgCl) and small Tafel slope of 48 mV/decade in 1 M KOH solution. That illustrates that the as-synthesized mesoporous Co_3O_4 is an efficient catalyst for OER. Meanwhile, the mesoporous Co_3O_4 exhibits good catalytic stability during OER. This can be attributed to both the stability of the unique mesoporous structure and highly reactive facets.

■ ASSOCIATED CONTENT

Supporting Information

Nitrogen adsorption and desorption isotherms of intermediate $Co(CO_3)_{0.5}(OH)_{0.11}H_2O$, SEM images, electrochemical impedance spectra, and ex-situ SEM images after the test of mesoporous Co_3O_4 nanoflakes are provided. This material is available free of charge via the Internet at http://pubs.acs.org.

■ AUTHOR INFORMATION

Corresponding Authors

*E-mail: neilchensq@gmail.com.
*E-mail: Guoxiu.Wang@uts.edu.au.

Author Contributions

S.C. and G.W. designed and conceived the idea. S.C. synthesized and characterized the samples. Y.Z. assisted in testing OER measurements. Z.A. did the theoretical calculation. B.S., X.X. and Y.W. participated in the discussion of the results. S.C. wrote the manuscript. G.W. revised the manuscript. All authors have given approval to the final version of the manuscript.

Funding

This project is financially supported by the Australian Research Council (ARC) through the ARC Discovery project (DP1093855) and ARC Future Fellowship project (FT110100800), The Fundamental Research Funds for the Central University of China (NE2014301), and partially supported from the China Scholarship Council (CSC, No. 2011689009).

Notes

The authors declare no competing financial interest.

■ ACKNOWLEDGMENTS

We appreciate and acknowledge the support from the Australian Research Council (ARC) and the ARC Future Fellowship project as well as the China Scholarship Council.

■ REFERENCES

(1) Cheng, F. Y.; Liang, J.; Tao, Z. L.; Chen, J. Functional Materials for Rechargeable Batteries. *Adv. Mater.* **2011**, *23*, 1695−1715.
(2) Liu, J. Addressing the Grand Challenges in Energy Storage. *Adv. Funct. Mater.* **2013**, *23*, 924−928.
(3) Chen, S.; Bao, P.; Xiao, L.; Wang, G. Large-Scale and Low Cost Synthesis of Graphene as High Capacity Anode Materials for Lithium-Ion Batteries. *Carbon* **2013**, *64*, 158−169.
(4) Chen, S.; Yeoh, W.; Liu, Q.; Wang, G. Chemical-free Synthesis of Graphene−Carbon Nanotube Hybrid Materials for Reversible Lithium Storage in Lithium-ion Batteries. *Carbon* **2012**, *50*, 4557−4565.
(5) Chen, S.; Wang, Y.; Ahn, H.; Wang, G. Microwave Hydrothermal Synthesis of High Performance Tin−Graphene Nanocomposites for Lithium Ion Batteries. *J. Power Sources* **2012**, *216*, 22−27.
(6) Mondal, A. K.; Wang, B.; Su, D.; Wang, Y.; Chen, S.; Zhang, X.; Wang, G. Graphene/MnO_2 Hybrid Nanosheets as High Performance Electrode Materials for Supercapacitors. *Mater. Chem. Phys.* **2014**, *143*, 740−746.
(7) Chen, S.; Chen, P.; Wang, Y. Carbon Nanotubes Grown in situ on Graphene Nanosheets as Superior Anodes for Li-ion Batteries. *Nanoscale* **2011**, *3*, 4323−9.
(8) Chen, S.; Bao, P.; Huang, X.; Sun, B.; Wang, G. Hierarchical 3D Mesoporous Silicon@Graphene Nanoarchitectures for Lithium Ion Batteries with Superior Performance. *Nano Res.* **2014**, *7*, 85−94.
(9) Yao, Y.; McDowell, M. T.; Ryu, I.; Wu, H.; Liu, N.; Hu, L.; Nix, W. D.; Cui, Y. Interconnected Silicon Hollow Nanospheres for Lithium-Ion Battery Anodes with Long Cycle Life. *Nano Lett.* **2011**, *11*, 2949−2954.
(10) Wang, Y.; Zeng, H. C.; Lee, J. Y. Highly Reversible Lithium Storage in Porous SnO_2 Nanotubes with Coaxially Grown Carbon Nanotube Overlayers. *Adv. Mater.* **2006**, *18*, 645−649.
(11) Wang, Y.; Lee, J. Y.; Chen, B. H. Microemulsion Syntheses of Sn and SnO_2-Graphite Nanocomposite Anodes for Li-ion Batteries. *J. Electrochem. Soc.* **2004**, *151*, A563−A570.
(12) Chen, S.; Chen, P.; Wu, M.; Pan, D.; Wang, Y. Graphene Supported Sn−Sb@Carbon Core-shell Particles as a Superior Anode for Lithium Ion Batteries. *Electrochem. Commun.* **2010**, *12*, 1302−1306.
(13) Huang, X. H.; Tu, J. P.; Xia, X. H.; Wang, X. L.; Xiang, J. Y.; Zhang, L.; Zhou, Y. Morphology Effect on the Electrochemical Performance of NiO Films as Anodes for Lithium Ion Batteries. *J. Power Sources* **2009**, *188*, 588−591.
(14) Lukowski, M. A.; Jin, S. Improved Synthesis and Electrical Properties of Si-Doped α-Fe_2O_3 Nanowires. *J. Phys. Chem. C* **2011**, *115*, 12388−12395.
(15) Wu, F. D.; Wang, Y. Self-assembled Echinus-like Nanostructures of Mesoporous CoO Nanorod@CNT for Lithium-ion Batteries. *J. Mater. Chem.* **2011**, *21*, 6636−6641.
(16) Bai, S.; Chen, S.; Shen, X.; Zhu, G.; Wang, G. Nanocomposites of Hematite ([small alpha]-Fe_2O_3) Nanospindles with Crumpled Reduced Graphene Oxide Nanosheets as High-performance Anode Material for Lithium-ion Batteries. *RSC Adv.* **2012**, *2*, 10977−10984.
(17) Huang, X.; Sun, B.; Chen, S.; Wang, G. Self-Assembling Synthesis of Free-standing Nanoporous Graphene−Transition-Metal Oxide Flexible Electrodes for High-Performance Lithium-Ion Batteries and Supercapacitors. *Chem.—Asian J.* **2014**, *9*, 206−211.
(18) Chen, S. Q.; Wang, Y. Microwave-assisted Synthesis of a Co_3O_4−Graphene Sheet-on-sheet Nanocomposite as a Superior Anode Material for Li-ion Batteries. *J. Mater. Chem.* **2010**, *20*, 9735−9739.
(19) Zhuang, Z.; Sheng, W.; Yan, Y. Synthesis of Monodispere Au@Co_3O_4 Core-Shell Nanocrystals and Their Enhanced Catalytic Activity for Oxygen Evolution Reaction. *Adv. Mater.* **2014**, *26*, 3950−3955.
(20) Koza, J. A.; He, Z.; Miller, A. S.; Switzer, J. A. Electrodeposition of Crystalline Co_3O_4—A Catalyst for the Oxygen Evolution Reaction. *Chem. Mater.* **2012**, *24*, 3567−3573.
(21) Fan, Y.; Shao, G.; Ma, Z.; Wang, G.; Shao, H.; Yan, S. Ultrathin Nanoflakes Assembled 3D Hierarchical Mesoporous Co_3O_4 Nanoparticles for High-Rate Pseudocapacitors. *Part. Part. Syst. Charact.* **2014**, *31*, 1079−1083.
(22) Zeng, J.; Francia, C.; Amici, J.; Bodoardo, S.; Penazzi, N. Mesoporous Co_3O_4 Nanocrystals as an Effective Electro-Catalyst for Highly Reversible Li−O_2 Batteries. *J. Power Sources* **2014**, *272*, 1003−1009.
(23) Wu, Z.-S.; Ren, W.; Wen, L.; Gao, L.; Zhao, J.; Chen, Z.; Zhou, G.; Li, F.; Cheng, H.-M. Graphene Anchored with Co_3O_4 Nanoparticles as Anode of Lithium Ion Batteries with Enhanced Reversible Capacity and Cyclic Performance. *ACS Nano* **2010**, *4*, 3187−3194.

DOI: 10.1021/am508136k
ACS Appl. Mater. Interfaces 2015, 7, 3306−3313

(24) Liu, Y.; Mi, C.; Su, L.; Zhang, X. Hydrothermal Synthesis of Co_3O_4 Microspheres as Anode Material for Lithium-Ion Batteries. *Electrochim. Acta* **2008**, *53*, 2507−2513.
(25) Sun, H.; Xin, G.; Hu, T.; Yu, M.; Shao, D.; Sun, X.; Lian, J. High-Rate Lithiation-Induced Reactivation of Mesoporous Hollow Spheres for Long-Lived Lithium-Ion Batteries. *Nat. Commun.* **2014**, *5*, 4526.
(26) Sun, H.; Sun, X.; Hu, T.; Yu, M.; Lu, F.; Lian, J. Graphene-Wrapped Mesoporous Cobalt Oxide Hollow Spheres Anode for High-Rate and Long-Life Lithium Ion Batteries. *J. Phys. Chem. C* **2014**, *118*, 2263−2272.
(27) Lai, L.; Zhu, J.; Li, Z.; Yu, D. Y. W.; Jiang, S.; Cai, X.; Yan, Q.; Lam, Y. M.; Shen, Z.; Lin, J. Co_3O_4/Nitrogen Modified Graphene Electrode as Li-ion Battery Anode with High Reversible Capacity and Improved Initial Cycle Performance. *Nano Energy* **2014**, *3*, 134−143.
(28) Liu, D.; Wang, X.; Wang, X.; Tian, W.; Bando, Y.; Golberg, D. Co_3O_4 Nanocages with Highly Exposed {110} Facets for High-Performance Lithium Storage. *Sci. Rep.* **2013**, *3*, 2543.
(29) Lou, X. W.; Deng, D.; Lee, J. Y.; Feng, J.; Archer, L. A. Self-Supported Formation of Needlelike Co_3O_4 Nanotubes and Their Application as Lithium-Ion Battery Electrodes. *Adv. Mater.* **2008**, *20*, 258−262.
(30) Lou, X. W.; Deng, D.; Lee, J. Y.; Archer, L. A. Thermal Formation of Mesoporous Single-Crystal Co_3O_4 Nano-Needles and Their Lithium Storage Properties. *J. Mater. Chem.* **2008**, *18*, 4397−4401.
(31) Du, N.; Zhang, H.; Chen, B. D.; Wu, J. B.; Ma, X. Y.; Liu, Z. H.; Zhang, Y. Q.; Yang, D. R.; Huang, X. H.; Tu, J. P. Porous Co_3O_4 Nanotubes Derived From $Co_4(CO)_{12}$ Clusters on Carbon Nanotube Templates: A Highly Efficient Material For Li-Battery Applications. *Adv. Mater.* **2007**, *19*, 4505−4509.
(32) Jeong, S.; Park, S.; Cho, J. High-Performance, Layered, 3D-$LiCoO_2$ Cathodes with a Nanoscale Co_3O_4 Coating via Chemical Etching. *Adv. Energy Mater.* **2011**, *1*, 368−372.
(33) Zhang, G.; Wang, T.; Yu, X.; Zhang, H.; Duan, H.; Lu, B. Nanoforest of Hierarchical Co_3O_4@$NiCo_2O_4$ Nanowire Arrays for High-Performance Supercapacitors. *Nano Energy* **2013**, *2*, 586−594.
(34) Gao, M.-R.; Xu, Y.-F.; Jiang, J.; Zheng, Y.-R.; Yu, S.-H. Water Oxidation Electrocatalyzed by an Efficient Mn_3O_4/$CoSe_2$ Nanocomposite. *J. Am. Chem. Soc.* **2012**, *134*, 2930−2933.
(35) Cowin, P. I.; Petit, C. T. G.; Lan, R.; Irvine, J. T. S.; Tao, S. Recent Progress in the Development of Anode Materials for Solid Oxide Fuel Cells. *Adv. Energy Mater.* **2011**, *1*, 314−332.
(36) Masa, J.; Xia, W.; Sinev, I.; Zhao, A.; Sun, Z.; Grützke, S.; Weide, P.; Muhler, M.; Schuhmann, W. Mn_xO_y/NC and Co_xO_y/NC Nanoparticles Embedded in a Nitrogen-Doped Carbon Matrix for High-Performance Bifunctional Oxygen Electrodes. *Angew. Chem., Int. Ed.* **2014**, *53*, 8508−8512.
(37) Ma, T. Y.; Dai, S.; Jaroniec, M.; Qiao, S. Z. Graphitic Carbon Nitride Nanosheet−Carbon Nanotube Three-Dimensional Porous Composites as High-Performance Oxygen Evolution Electrocatalysts. *Angew. Chem., Int. Ed.* **2014**, *53*, 7281−7285.
(38) Cheng, Y.; Liu, C.; Cheng, H.-M.; Jiang, S. P. One-Pot Synthesis of Metal−Carbon Nanotubes Network Hybrids as Highly Efficient Catalysts for Oxygen Evolution Reaction of Water Splitting. *ACS Appl. Mater. Interfaces* **2014**, *6*, 10089−10098.
(39) Wang, L.; Lin, C.; Huang, D.; Zhang, F.; Wang, M.; Jin, J. A Comparative Study of Composition and Morphology Effect of $NixCo_1-x(OH)_2$ on Oxygen Evolution/Reduction Reaction. *ACS Appl. Mater. Interfaces* **2014**, *6*, 10172−10180.
(40) Ge, X.; Liu, Y.; Goh, F. W. T.; Hor, T. S. A.; Zong, Y.; Xiao, P.; Zhang, Z.; Lim, S. H.; Li, B.; Wang, X.; Liu, Z. Dual-Phase Spinel $MnCo_2O_4$ and Spinel $MnCo_2O_4$/Nanocarbon Hybrids for Electrocatalytic Oxygen Reduction and Evolution. *ACS Appl. Mater. Interfaces* **2014**, *6*, 12684−12691.
(41) Liang, Y.; Wang, H.; Diao, P.; Chang, W.; Hong, G.; Li, Y.; Gong, M.; Xie, L.; Zhou, J.; Wang, J.; Regier, T. Z.; Wei, F.; Dai, H. Oxygen Reduction Electrocatalyst Based on Strongly Coupled Cobalt Oxide Nanocrystals and Carbon Nanotubes. *J. Am. Chem. Soc.* **2012**, *134*, 15849−15857.
(42) Pickrahn, K. L.; Park, S. W.; Gorlin, Y.; Lee, H.-B.-R.; Jaramillo, T. F.; Bent, S. F. Active MnO_x Electrocatalysts Prepared by Atomic Layer Deposition for Oxygen Evolution and Oxygen Reduction Reactions. *Adv. Energy Mater.* **2012**, *2*, 1269−1277.
(43) Ma, T. Y.; Dai, S.; Jaroniec, M.; Qiao, S. Z. Metal−Organic Framework Derived Hybrid Co_3O_4-Carbon Porous Nanowire Arrays as Reversible Oxygen Evolution Electrodes. *J. Am. Chem. Soc.* **2014**, *136*, 13925−13931.
(44) Esswein, A. J.; McMurdo, M. J.; Ross, P. N.; Bell, A. T.; Tilley, T. D. Size-Dependent Activity of Co_3O_4 Nanoparticle Anodes for Alkaline Water Electrolysis. *J. Phys. Chem. C* **2009**, *113*, 15068−15072.
(45) Wu, J.; Xue, Y.; Yan, X.; Yan, W.; Cheng, Q.; Xie, Y. Co_3O_4 Nanocrystals on Single-Walled Carbon Nanotubes as a Highly Efficient Oxygen-Evolving Catalyst. *Nano Res.* **2012**, *5*, 521−530.
(46) Wang, Y.; Zhang, H. J.; Wei, J.; Wong, C. C.; Lin, J.; Borgna, A. Crystal-Match Guided Formation of Single-Crystal Tricobalt Tetraoxygen Nanomesh as Superior Anode for Electrochemical Energy Storage. *Energy Environ. Sci.* **2011**, *4*, 1845−1854.
(47) Farhadi, S.; Pourzare, K.; Sadeghinejad, S. Simple Preparation of Ferromagnetic Co_3O_4 Nanoparticles by Thermal Dissociation of the $[CoII(NH_3)_6](NO_3)_2$ Complex at Low Temperature. *J. Nanostruct. Chem.* **2013**, *3*, 1−7.
(48) Zhang, Q.; Zhao, M.-Q.; Tang, D.-M.; Li, F.; Huang, J.-Q.; Liu, B.; Zhu, W.-C.; Zhang, Y.-H.; Wei, F. Carbon-Nanotube-Array Double Helices. *Angew. Chem., Int. Ed.* **2010**, *49*, 3642−3645.
(49) Lu, Y.; Wang, Y.; Zou, Y.; Jiao, Z.; Zhao, B.; He, Y.; Wu, M. Macroporous Co_3O_4 Platelets with Excellent Rate Capability as Anodes for Lithium Ion Batteries. *Electrochem. Commun.* **2010**, *12*, 101−105.
(50) Zou, X.; Su, J.; Silva, R.; Goswami, A.; Sathe, B. R.; Asefa, T. Efficient Oxygen Evolution Reaction Catalyzed by Low-Density Ni-Doped Co_3O_4 Nanomaterials Derived from Metal-Embedded Graphitic C_3N_4. *Chem. Commun.* **2013**, *49*, 7522−7524.
(51) Wang, D.; Chen, X.; Evans, D. G.; Yang, W. Well-Dispersed Co_3O_4/Co_2MnO_4 Nanocomposites as a Synergistic Bifunctional Catalyst for Oxygen Reduction and Oxygen Evolution Reactions. *Nanoscale* **2013**, *5*, 5312−5315.
(52) Wang, Y.; Cui, X.; Chen, L.; Wei, C.; Cui, F.; Yao, H.; Shi, J.; Li, Y. One-Step Replication and Enhanced Catalytic Activity for Cathodic Oxygen Reduction of the Mesostructured Co_3O_4/Carbon Composites. *Dalton Trans.* **2014**, *43*, 4163−4168.
(53) Liang, Y.; Li, Y.; Wang, H.; Zhou, J.; Wang, J.; Regier, T.; Dai, H. Co_3O_4 Nanocrystals on Graphene as a Synergistic Catalyst for Oxygen Reduction Reaction. *Nat. Mater.* **2011**, *10*, 780−786.
(54) Singh, R. N.; Hamdani, M.; Koenig, J. F.; Poillerat, G.; Gautier, J. L.; Chartier, P. Thin Films of Co_3O_4 and $NiCo_2O_4$ Obtained by the Method of Chemical Spray Pyrolysis for Electrocatalysis III. The Electrocatalysis of Oxygen Evolution. *J. Appl. Electrochem.* **1990**, *20*, 442−446.
(55) Wang, Y.; Zhou, T.; Jiang, K.; Da, P.; Peng, Z.; Tang, J.; Kong, B.; Cai, W.-B.; Yang, Z.; Zheng, G. Reduced Mesoporous Co_3O_4 Nanowires as Efficient Water Oxidation Electrocatalysts and Supercapacitor Electrodes. *Adv. Energy Mater.* **2014**, *4*, 1400696.
(56) Zhou, W.; Wu, X.-J.; Cao, X.; Huang, X.; Tan, C.; Tian, J.; Liu, H.; Wang, J.; Zhang, H. Ni_3S_2 Nanorods/Ni Foam Composite Electrode with Low Overpotential for Electrocatalytic Oxygen Evolution. *Energy Environ. Sci.* **2013**, *6*, 2921−2924.
(57) Liao, L.; Zhu, J.; Bian, X.; Zhu, L.; Scanlon, M. D.; Girault, H. H.; Liu, B. MoS_2 Formed on Mesoporous Graphene as a Highly Active Catalyst for Hydrogen Evolution. *Adv. Funct. Mater.* **2013**, *23*, 5326−5333.
(58) Chen, S.; Duan, J.; Jaroniec, M.; Qiao, S. Z. Three-Dimensional N-Doped Graphene Hydrogel/NiCo Double Hydroxide Electrocatalysts for Highly Efficient Oxygen Evolution. *Angew. Chem., Int. Ed.* **2013**, *52*, 13567−13570.

DOI: 10.1021/am508136k
ACS Appl. Mater. Interfaces 2015, 7, 3306−3313